Hindawi
Advances in Civil Engineering
Volume 2019, Article ID 7318768, 14 pages
https://doi.org/10.1155/2019/7318768

Research Article

Effect of Hydrothermal Coupling on Physical and Dynamic Mechanical Properties of Sandstone

Rong-rong Zhang[1,2,3] **and Pu Yuan**[1,2,3,4]

[1]*Research Center of Mine Underground Engineering, Ministry of Education, Anhui University of Science and Technology, Huainan, Anhui 232001, China*
[2]*School of Civil Engineering and Architecture, Anhui University of Science and Technology, Huainan, Anhui 232001, China*
[3]*State Key Laboratory of Mining Response and Disaster Prevention and Control in Deep Coal Mine, Anhui University of Science and Technology, Huainan, Anhui 232001, China*
[4]*Department of Civil, Construction, and Environmental Engineering, The University of Alabama, Tuscaloosa, AL 35487, USA*

Correspondence should be addressed to Pu Yuan; puy2012@126.com

Received 4 December 2018; Revised 12 February 2019; Accepted 19 February 2019; Published 1 April 2019

Academic Editor: Emanuele Brunesi

Split-Hopkinson pressure bar (SHPB) tests were conducted for sandstone after recurrent heat-cool (H-C) cycles. Physical and mechanical properties, damage, and fracture characteristics of sandstone after the H-C cycle were explored. Additionally, the damage variable and release rate of damage strain were defined to describe the damage degree of the sandstone specimen after recurrent H-C cycles. Finally, the relationship between mass fractal dimension of fragmentation and cycling number was discussed. Results show that the P-wave velocity and density decrease with the increase of cycling number, while the porosity increases. It was found that the dynamic compressive strength and relative elastic modulus decrease with the increase of cycling number. 20 cycles is the critical point for the low temperature (L-T) group and moderate temperature (M-T) group, while it is 4 cycles for the high temperature (H-T) group. With the increase of cycling number, both the damage variable and release rate of damage strain of rock increase, while the destruction degree of sandstone becomes greater, and the corresponding fragments show more evenly.

1. Introduction

Heat-cool (H-C) cycle is a typical weathering process, which shows strong effect on the physical and mechanical properties of rock. Rock weathering is a phenomenon of rock breakage, porosity, and secondary change of mineral composition under the combined action of solar radiation, atmosphere, water, or biology [1, 2]. The recurrent H-C cycles cause degradation of rock engineering [3, 4]; in addition, because of the widely existed volcano eruption, thermal shock, exploitation of geothermal resources, and deep geological repositories for heat-generating radioactive wastes, which have significant effects on degradation degree of rocks, should be considered as an important factor in the H-C cycle process. In addition, the rock is not only in the environment of hydrothermal coupling in the underground and ground engineering but also subjected to the effects of engineering disturbance, earthquake, and other impact loads in the whole construction and operation process [5]. Recurrent H-C cycles lead to changes in the microstructure of rocks, which cause generation of new microcracks and micropores inside rocks [3, 6–8]. Rock tends to experience a deep weathering due to repeated erosion of water and temperature. Resistance ability of the rock to the H-C cycle depends on a complex set of material properties, including mineralogical composition, inner structure, and pore characteristics of rock [9]. When the temperature floats down the freezing point of water, a 9% volume expansion occurs inside rock, which causes damage to rock caused by great ice pressure. The frequent freeze-thaw (F-T) of water expands the original fissures inside rock. The freeze-thaw phenomenon also induces new microcracks in rock, which causes great damage to rock engineering [10–12]. Due to various coefficients for different mineral particles, temperature increment during the H-C cycle leads to secondary thermal stress in rock. Studies show that the main mechanism of H-C cycles on rock is the loss of water and

damage of the inner structure caused by thermal reactions [13–15].

Weathered rock is damaged not only by water and temperature but also subject to dynamic loads, such as blasting, mechanized construction, and earthquake vibration [16, 17]. However, by summarizing the theoretical and experimental studies achievements of predecessors, it can be found that researches, in terms of the physical and mechanical changes of rock during the weathering process, mainly concentrate on the static mechanical properties and physical characteristics. Less research has concentrated on the study for the dynamic mechanical properties of weathered rock. Ma et al. [18] investigate the effects of F-T cycles on dynamic compressive strength and energy distribution parameters for soft rock. Wang et al. [19] compared the static and dynamic mechanical characteristic of red sandstone free from and after F-T or thermal shock (T-S) weathering. Test results show that both the static and dynamic strength of rock after F-T or T-S cycles decrease compared with that of fresh specimen; additionally, the decrease degree of the dynamic property induced by F-T or T-S cycles is larger than that under static loads. Xu and Dai [20] studied the dynamic response and failure mechanism of brittle rock under compression-shear combined loading and proposed a new method to describe the mechanical response and failure mechanism of brittle rock under dynamic compression-shear loading. Du et al. [21] accurately describe characterization of the strength and failure behavior of deep rock under coupled hydrostatic confinement and dynamic loading in the deep underground engineering. The discrete element method (DEM) is used. This study systematically investigates the mechanical behavior of granite specimens under different hydrostatic confinements in the split-Hopkinson compression bar (SHPB) test, which provides an important guarantee for engineering safety. Very little research work has been conducted on the dynamic property of rock after H-C cycles, especially for rock after the H-C cycle with different heat temperatures. On the earth's surface, 70% of the rock is sedimentary rock, which accounts for 80% of the total mineral deposits in the world. Sandstone is a sedimentary rock formed by sand-sized grains. Therefore, sandstone is selected as the test sample, SHPB tests are carried out for sandstone after H-C cycles with different heat temperatures (e.g., 50, 100, and 400°C), and the objective of this research work is to investigate the effect of H-C cycles on the deterioration of physical and dynamic mechanical properties, such as porosity, P-wave velocity, density, dynamic strength, elastic modulus, and failure mode. The damage variable and release rate of damage strain energy are defined to describe the damage degree of rock after recurrent H-C cycles. Finally, the relationship between mass fractal dimension of fragmentation and cycling number is studied.

2. Specimen Preparation and Experimental Setup

2.1. Sample Preparation. Fine-grained sandstone samples were collected from the Zhujidong coalmine in Huainan city, Anhui province, China. Power X-ray diffraction analysis was adopted to study the mineral composition of rock at 20°C. According to the XRD spectrum (Figure 1), the

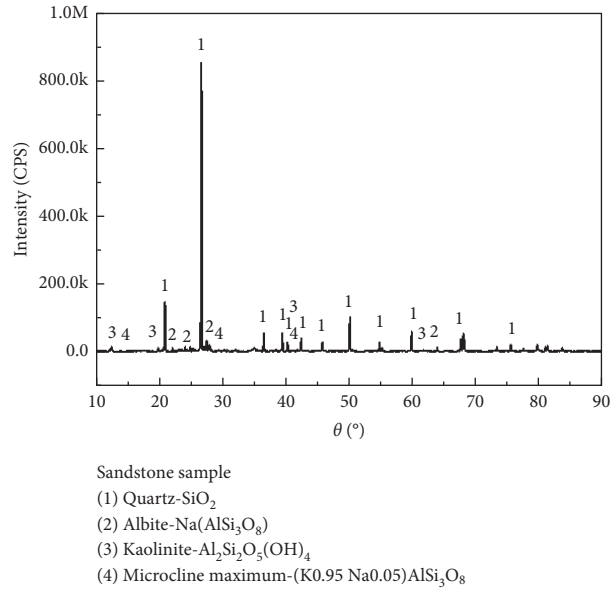

Figure 1: XRD spectrum of sandstone sample (under 20°C).

main components of sandstone are quartz accounted for 62.8%, besides of which the sandstone was composed of 12% albite, 6.98% kaolinite, and other minerals [22, 23]. As seen from Figures 2(a) and 2(b) and Table 1, the main elements of sandstone are Si, O, Ca, Fe, and Al. Scanning electron microscope (SEM) was performed on some offcuts of rock specimens, and chemical analyses were also conducted by energy dispersive spectroscopy (EDS). The primary fractures and pores were found by SEM. As seen from the EDS picture and Table 1, the brighter the color block, the more elements it contains, such as the relatively large numbers of elements in block 3. These primary fissures, pores, and elements have a significant effect on the physical and chemical properties of rocks. The SEM and EDS images of sandstone after different H-C cycles groups are shown in Figures 2(c)–2(h). It can be seen from the diagram that the cracks and pores in rocks increase with the increase of high temperature treatment temperature, showing a phenomenon of high temperature (H-T) group > moderate temperature (M-T) group > low temperature (L-T) group. Additionally, the above figures also illustrate that the damage degree of rock after 12 H-T cycles is obviously higher compared with that after M-T and L-T treatment. Samples with similar P-wave velocity were selected and processed into φ50 mm × 25 mm cylinder with surface parallelism within 0.05 mm and surface flatness within 0.02 mm. Sample processing dimensions and methods comply with the ISRM (International Society for Rock Mechanics) standard [24]. Surface planeness is controlled to ±0.05 mm, and the vertical deviation of the upper and lower surfaces is ±0.25°.

2.2. H-C Cycling and Testing Equipment. According to the heating temperature in H-C cycles, the test sandstone samples were divided into four groups: high temperature (H-T) group from −20°C to 400°C, moderate temperature

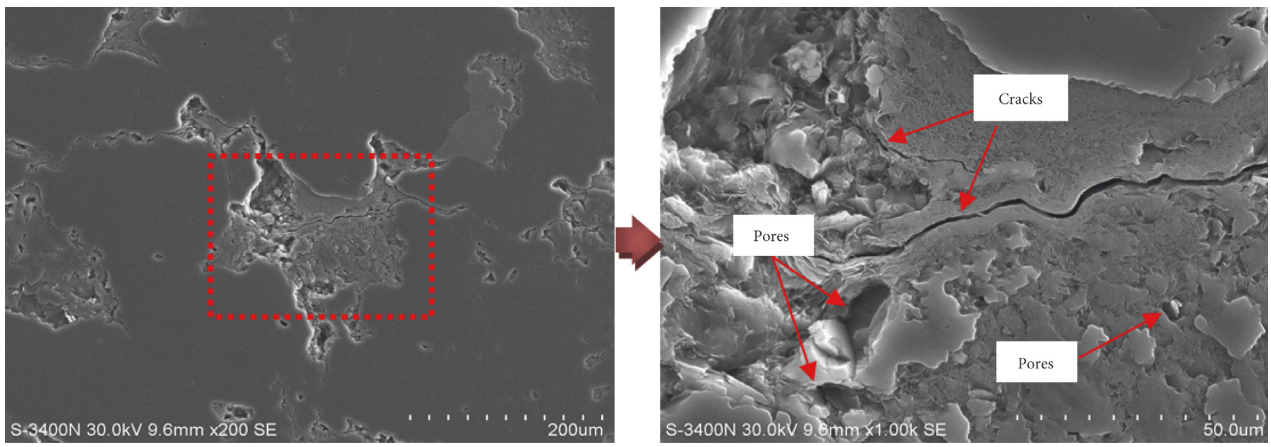

(a)

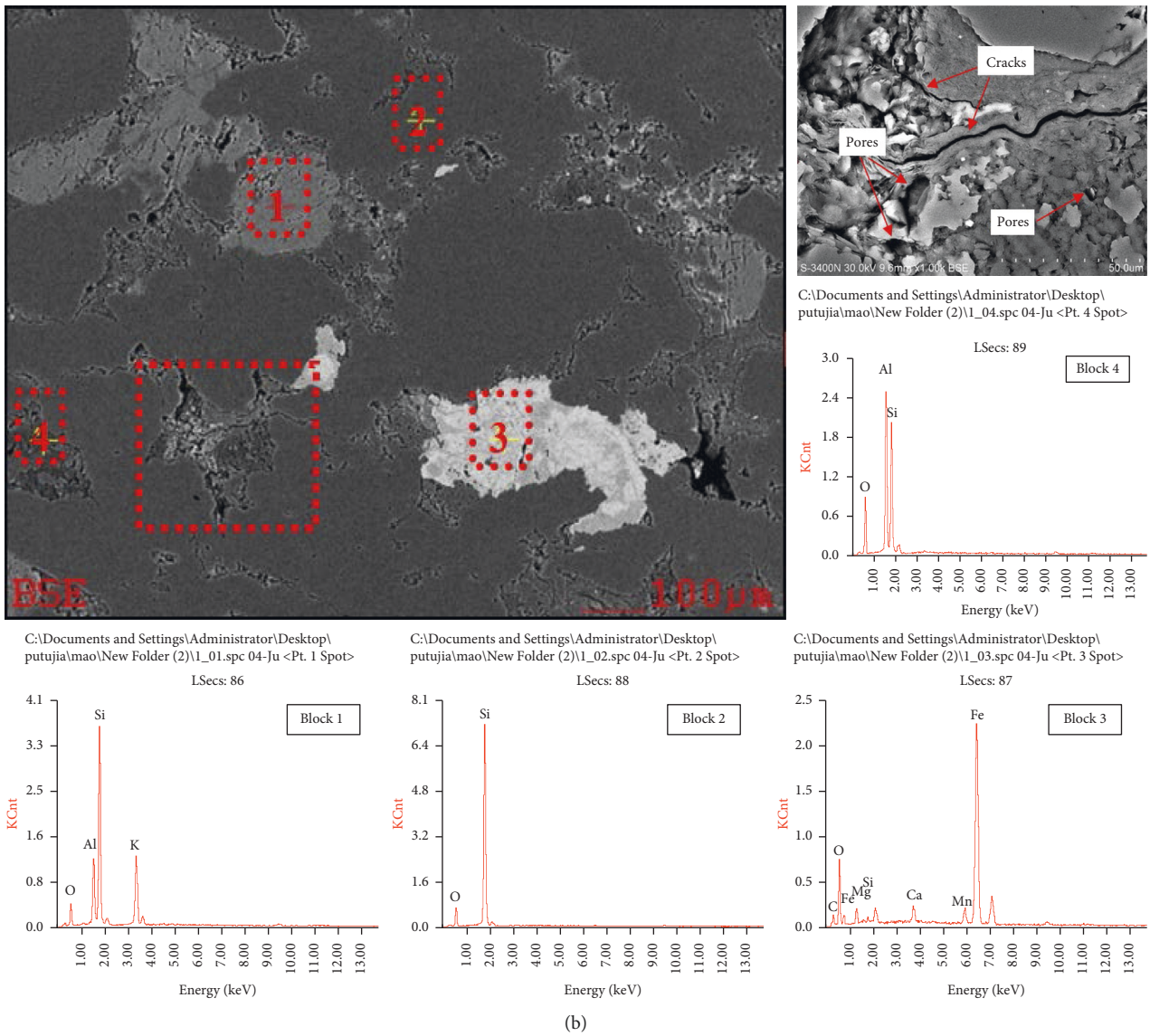

(b)

Figure 2: Continued.

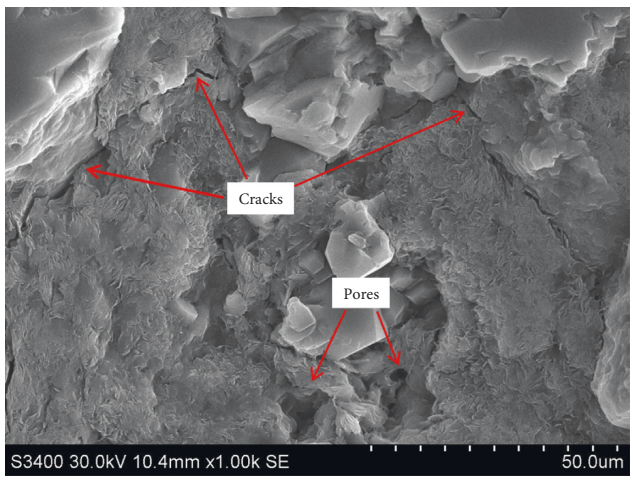

(c)

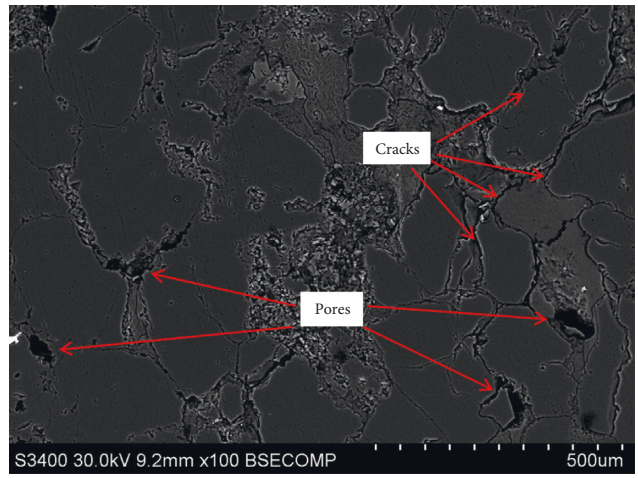

(d)

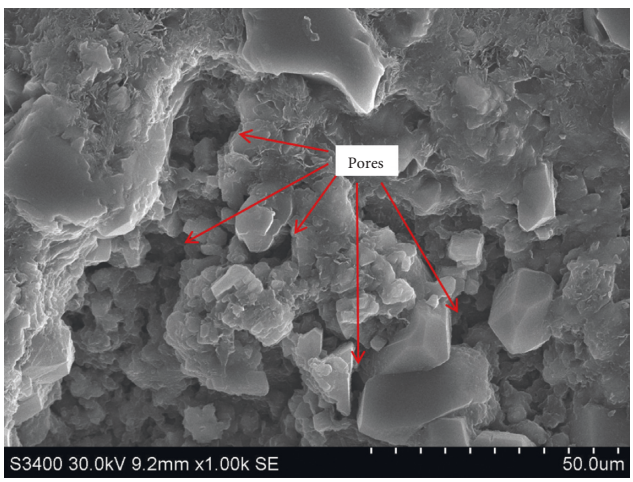

(e)

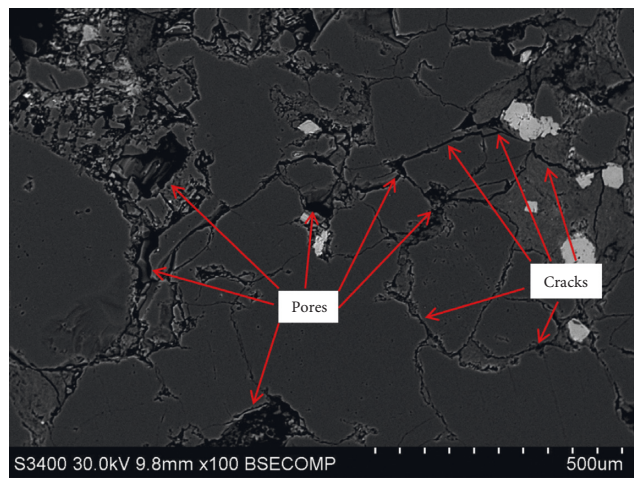

(f)

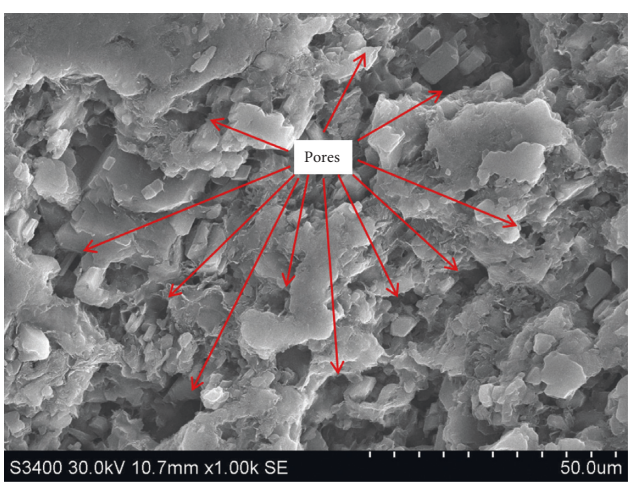

(g)

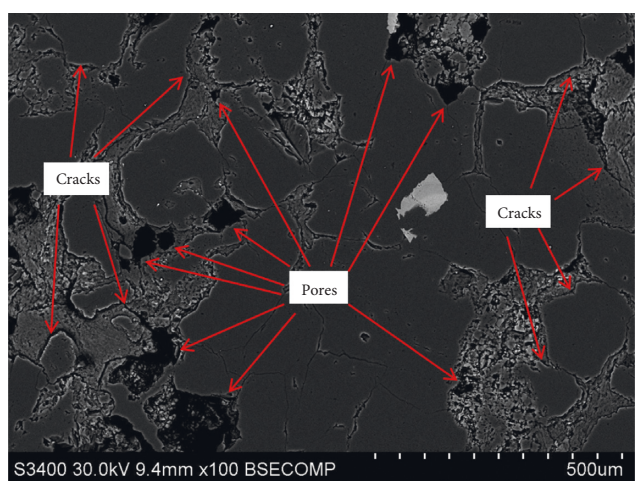

(h)

Figure 2: SEM and EDS observation of sandstone after H-C cycles: (a) 20°C (SEM 200 μm and 50 μm), (b) 20°C (EDS 100 μm), (c) after 40 cycles in L-T group (SEM 50 μm), (d) after 40 cycles in L-T group (EDS 500 μm), (e) after 40 cycles in M-T group (SEM 50 μm), (f) after 40 cycles in M-T group (EDS 500 μm), (g) after 12 cycles in H-T group (SEM 50 μm), and (h) after 12 cycles in H-T group (EDS 500 μm).

Table 1: wt.% and at.% of blocks in Figure 2(b).

Blocks in Figure 2(b)	Element	wt.%	at.%
1	O	29.51	43.93
	Al	11.90	10.50
	Si	41.35	35.06
	K	17.25	10.51
2	O	35.57	49.22
	Si	64.43	50.78
3	C	14.63	30.10
	O	25.74	39.76
	Mg	5.08	5.17
	Si	1.08	0.95
	Ca	1.93	1.19
	Mn	3.04	1.37
	Fe	48.5	21.47
4	O	40.33	53.83
	Al	26.02	20.59
	Si	33.65	25.59

(M-T) group from −20°C to 100°C, low temperature (L-T) group from −20°C to 50°C, and the control group (without H-C cycle). For L-T and M-T groups, 4 experimented sets are prepared according to 10, 20, 30, and 40 H-C cycles. Because of the fast deterioration rate of the high temperature group, 3 experimented sets are prepared according to 4, 8, and 12 H-C cycles. There are 5 specimens in each experimented set (Figure 3).

Heating device was a SX-5-12 box-type resistance furnace, which composes control box and electric furnace. The electric furnace could heat the specimens to a maximum temperature of 1200°C. Sandstone specimens were heated at a rate of 6°C/min to the desired temperature. The low-temperature test box was used in this test, and 40 min was needed for the test chamber to drop from 20°C to −20°C.

The whole H-C cycles process were shown as follows: sandstone samples were first immersed in water for 12 hours, then put them in a low-temperature test chamber at −20°C for 6 hours, and finally, heat samples in a high-temperature box at a predetermined temperature for 6 hours. A whole H-C cycle lasts for 24 h. The mass, volume, and P-wave velocity of sandstone samples were tested before and after different H-C cycles.

SHPB equipment has been successfully used to investigate the dynamic behaviors of materials, such as rock and concrete [25]. In this test, dynamic impact loading tests were conducted by the SHPB system with a diameter of 50 mm. As shown in Figure 4, it contains launch device, striker, incident bar, transmitted bar, buffer bar, and strain acquisition instrument, and two strain gauges are glued on the incident and transmitted bars to collect the origin strain signals; in addition, a striker with double-tapered shape was adopted to guarantee the stress balance of the rock specimen [26]. The SHPB test steps are as follows: (1) check all the test parts on the working state and adjust voltage balance, (2) appropriate lubricant is evenly smeared on the two side surfaces of the rock specimen and then put it between incident and transmitted bars, (3) open the gas pressure switch and collect the test signal, and (4) collect the fragment of the rock specimen. The dynamic stress-strain curves could be calculated according to the "three wave methods" [27–29]:

$$\sigma(t) = \frac{E_0 A_0}{2A_s}\left[\varepsilon_I(t) - \varepsilon_R(t) - \varepsilon_T(t)\right], \quad (1)$$

$$\varepsilon(t) = \frac{C_0}{l_s}\int_0^\tau \left[\varepsilon_I(t) - \varepsilon_R(t) - \varepsilon_T(t)\right]dt, \quad (2)$$

$$\dot{\varepsilon}(t) = \frac{C_0}{l_s}\left[\varepsilon_I(t) - \varepsilon_R(t) - \varepsilon_T(t)\right], \quad (3)$$

where $\varepsilon_I(t)$, $\varepsilon_R(t)$, and $\varepsilon_T(t)$ are the strain of incident wave, reflected wave, and transmitted wave, respectively; E_0, A_0, C_0, A_s, and l_s are Young's modulus, the cross-sectional area, the elastic wave speed of the bar, and the cross-sectional area, and the height of the rock specimen, respectively; and t is the duration time of the elastic wave. C_0 can be calculated by the following equation:

$$C_0 = \sqrt{\frac{E_0}{\rho_0}}, \quad (4)$$

where ρ_0 is the density of the bar material.

3. Test Results and Analysis

3.1. Variation in P-Wave Velocity. The P-wave velocity results of sandstone measured before and after different H-C cycles are shown in Figure 5. It can be noticed that before H-C cycles, the average wave velocities of the specimens range from 2870 m/s to 3067 m/s. For sandstone specimens after H-C cycles, it shows a decrease tendency of P-wave velocity. After 20 and 4 H-C cycles, the descent rate is relatively slow for L-T and M-T groups and the H-T group, respectively. The descent rate of P-wave velocity from 0 to 20 cycles is 7.93% and 11.52% for the L-T group and M-T group, respectively, while it is 41.09% for the H-T group from 0 to 4 cycles. As a contrast, after 20 cycles, the descent rates are only 1.91% and 4.42% for L-T and M-T groups, respectively, while the descent rate is only 19.42% for the H-T group from 4 to 12 cycles. Hence, 20 cycles is the critical point of P-wave velocity for the L-T group and M-T group, and 4 cycles is the critical point for the H-T group. There are two reasons for the variation of the P-wave velocity of sandstone. On the one hand, the water in the rock firstly absorbs water to attain saturation and then escapes because of the increase of temperature, which leads to the increase of pore volume due to the repeated absorption and escape of this kind of water. On the other hand, the generation and expansion of internal microcracks and micropores also lead to the attenuation of ultrasonic wave energy after rock damage.

3.2. Variation in Density and Porosity. Rock is naturally a three-phase system of air-water-solid, and rock density refers to the mass of rock in unit volume, which is significance for studying weathering process, stability of rock mass, and prediction of surrounding rock pressure in rock engineering [30]. By testing the volume and weight of rock

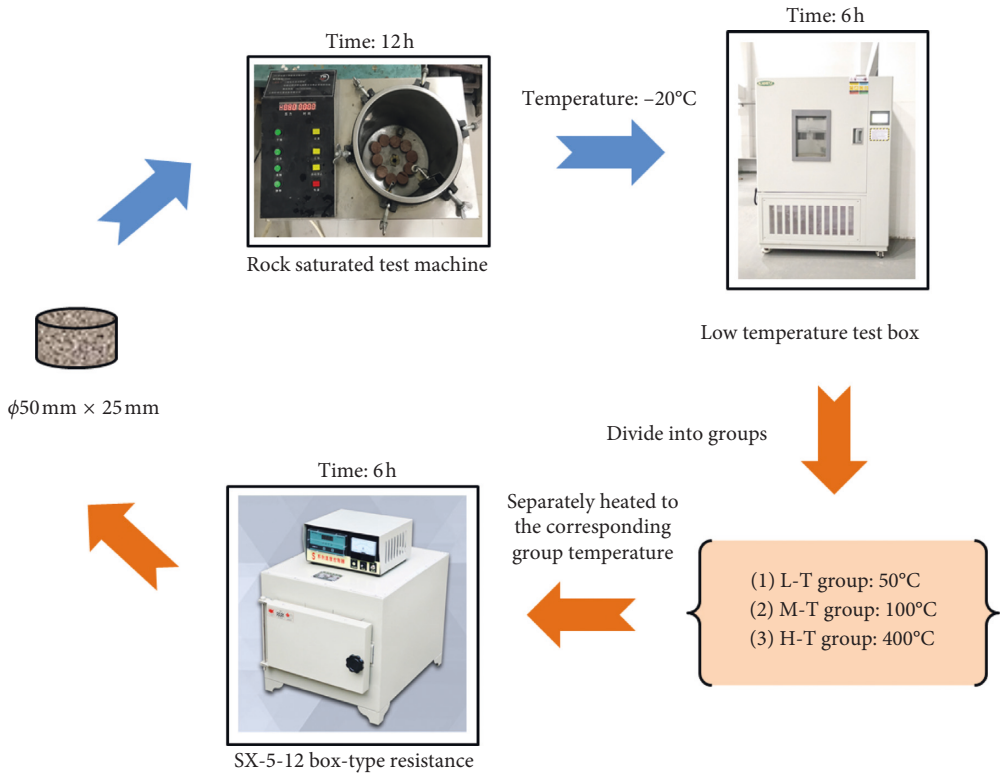

Figure 3: H-C cycles test procedure.

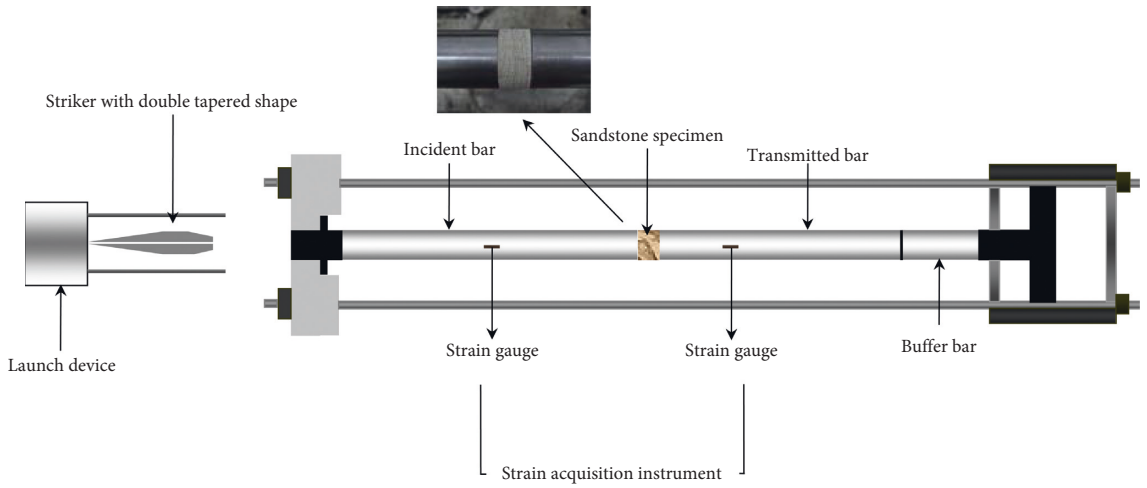

Figure 4: The functional diagram of SHPB.

samples before and after different H-C cycles, we obtained the variations in density with cycling number, as shown in Figure 6. It can be seen from the diagram that the density of sandstone samples gradually decreases with increasing cycling number for three groups.

Figure 6 also shows that the relationship between density and cycling number is similar to that of the P-wave velocity. The descent rates of density from 0 to 20 cycles are 1.14% and 1.80% for the L-T group and M-T group, respectively, while it is 2.44% for the H-T group from 0 to 4 cycles. After 20 cycles, the descent rates are only 0.27% and 0.33% for the L-T group and M-T group, respectively, while it has a 0.62% descent rate for the H-T group from 4 to 12 cycles. Hence, 20 cycles is the critical point of density for the L-T group and M-T group, and 4 cycles is the critical point for the H-T group.

Rock is a natural polycrystalline material with many defects and pores [31]. Porosity has great effect on the hydration and thermal and mechanical properties of rock and rock mass. The existence of pores makes it more vulnerable subject to external load, leading to further deterioration of rock. Therefore, the porosity change of rock

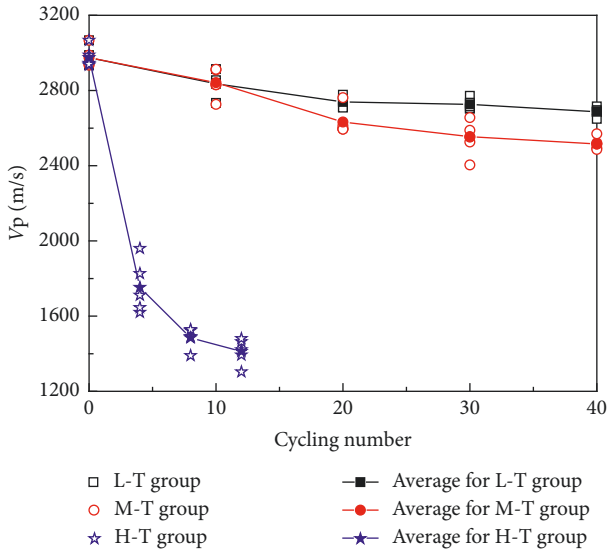

Figure 5: Test results of P-wave velocity for different groups before and after H-C cycles.

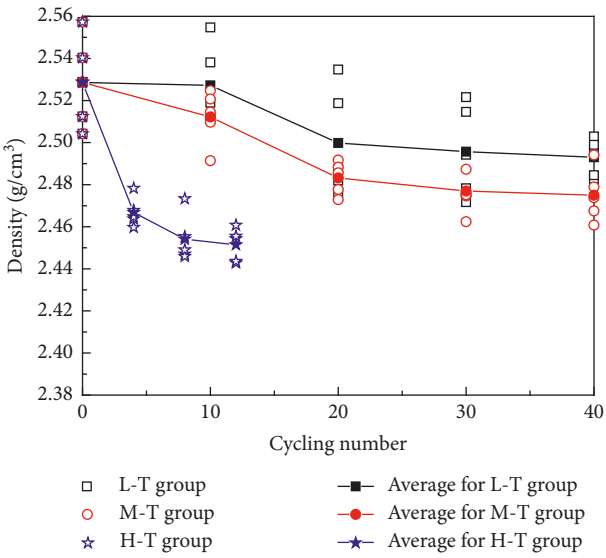

Figure 6: Variation of density of sandstone versus H-C cycles.

after different H-C cycles is measured and analyzed in this test.

Figure 7 illuminates the variation of porosity of sandstone versus H-C cycles. It is clearly notice that (1) under the same cycling number, the porosity of sandstone for the H-T group is much higher than that for L-T and M-T groups. (2) A different changing trend is found for three groups, and for L-T and M-T groups, with the increase of cycling number, the porosity exhibits a linear correlation. However, there shows a exponential growth relationship between porosity and cycling number for the H-T group, which attributes to the high temperature damage to the sandstone specimen. (3) The rise rate of porosity is higher from 0 to 20 cycles compared with that from 20 to 40 cycles for L-T and M-T groups, and the

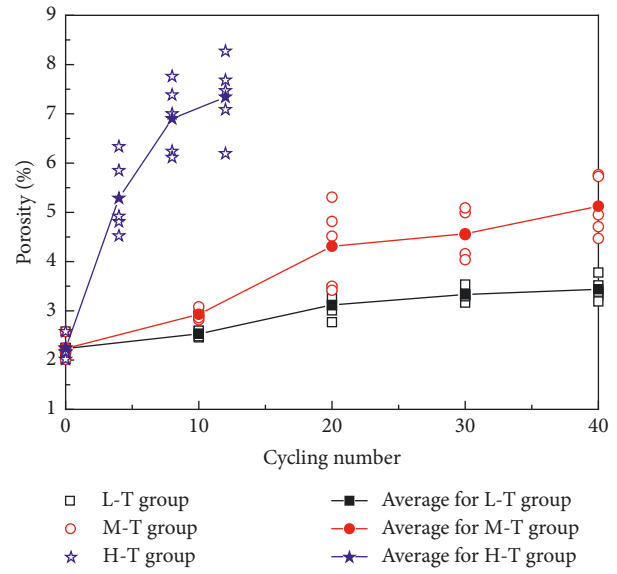

Figure 7: Variation of porosity of sandstone versus H-C cycles.

values of the rise rate of porosity from 0 to 20 cycles are 39.64% and 92.93% for L-T and M-T groups, respectively, while they are only 10.17% and 18.87% from 20 to 40 cycles. By contrast, the average value of porosity for the H-T group increases from 2.23% to 5.29% with the cycling number increasing from 0 to 4 cycles, with a 137.22% rise rate, while it changes from 5.29% to 7.34% when the cycling number increases from 4 to 12 cycles, with only 38.76% rise rate, which is much lower compared with that from 0 to 4 cycles.

3.3. Dynamic Stress-Strain Curve and Relative Elastic Modulus. Typical dynamic stress-strain curves are presented in Figure 8. By comparison of complete stress-strain curves of different groups, we can see that with the increase of axial strain, the stress increase rate gradually decreases with increasing cycling number before peak strain. The peak stress decreases with increasing cycling number. Furthermore, the brittleness of the sandstone samples gradually decreases and the ductility gradually increases as the increase of the cycling number.

The dynamic compressive strength is defined as the peak stress in the stress-strain curve in this research, and test results of dynamic compressive strength of the sandstone specimen at the strain rate of $(190 \pm 10)\ s^{-1}$ under different H-C cycles are shown in Figure 9(a).

Figure 9(a) results show that the dynamic compressive strength of rock decreases slowly after 40 cycles for L-T and M-T groups, while it decreases sharply after 4 cycles for H-T cycles. Specifically, the dynamic compressive strength of the control group is 143.17 MPa, and it only decreases to 103.80 MPa and 96.30 MPa after 40 cycles for L-T and M-T groups, respectively, and the corresponding descent rates are 27.50% and 32.74%, respectively. However, after 4 cycles for the H-T group, the dynamic compressive strength decreases to 64.38 MPa, with 55.03% descent rate, which is much larger than the other two groups.

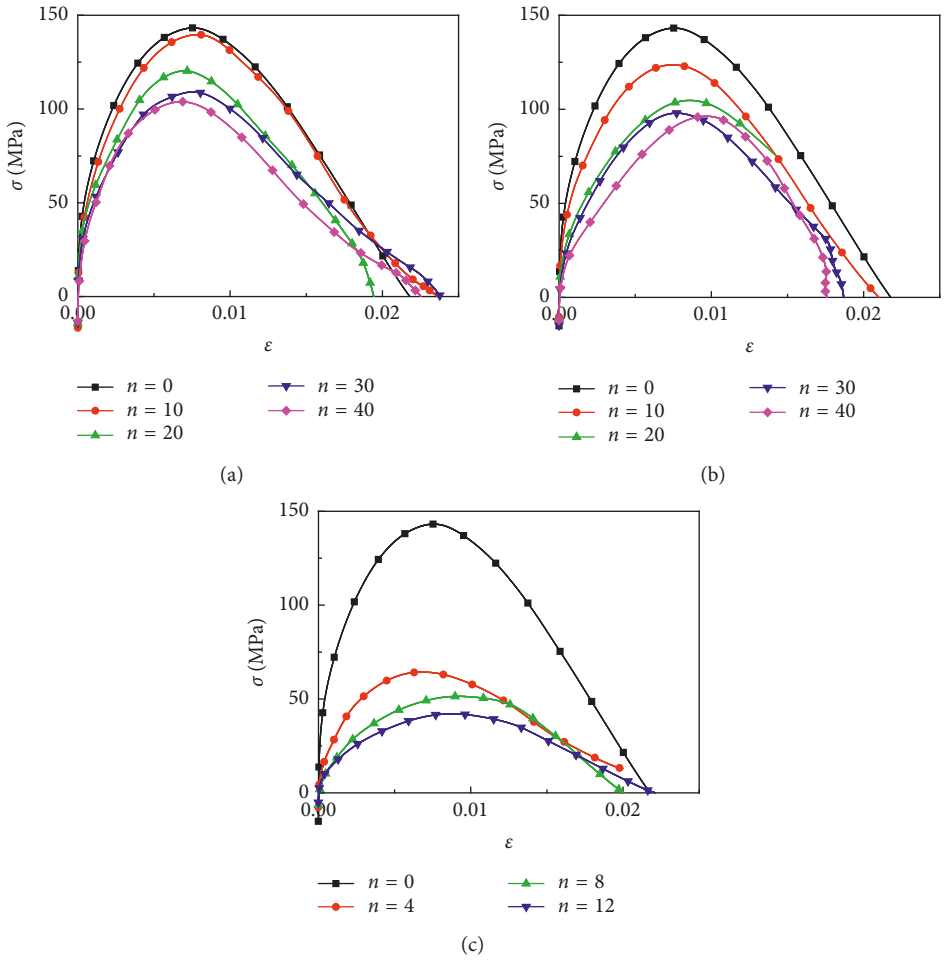

Figure 8: Dynamic stress-strain curve of sandstone specimens after H-C cycles: (a) L-T group, (b) M-T group, and (c) H-T group.

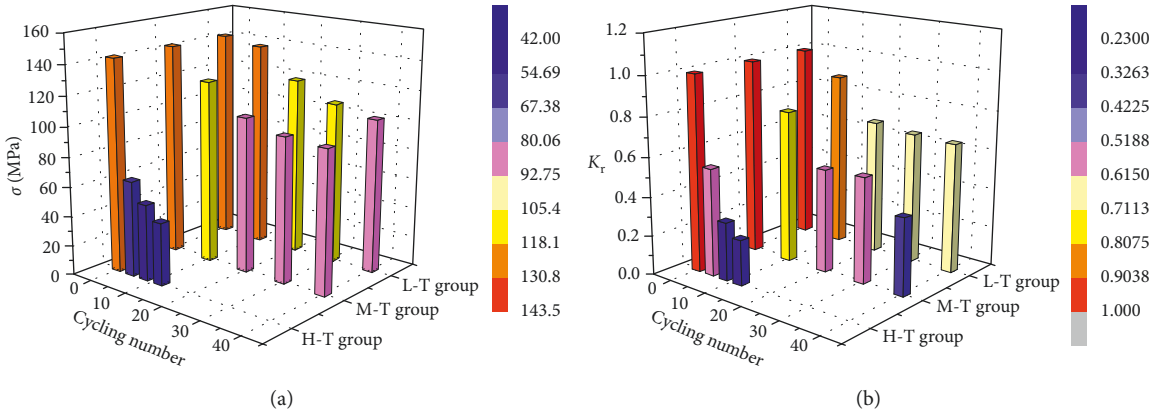

Figure 9: Effects of H-C cycles on peak stress and relative elastic modulus under different groups: (a) Relation of dynamic compressive strength with cycling number and (b) relation of relative elastic modulus with cycling number.

Elastic modulus in this research is defined as the slope corresponding to 40% and 60% of compression strength during the rising phase of the stress-strain curve; the calculated results are shown in Table 2. The results showed that the elastic modulus decreased with the increasing cycling number, in order to describe the drop degree of elastic modulus caused by the H-C cycle, the relative elastic modulus (K_r) is defined and can be calculated as follows:

Table 2: Test results on the basic dynamic properties of sandstone after H-C cycles.

Test number	Number of sample groups	Cycling number	Peak stress (MPa)	Elastic modulus (GPa)	Relative elastic modulus (K_r)
1	Room temperature	0	143.17	28.8	1.000
2	Low temperature (L-T) group	10	139.59	25.6	0.889
3		20	120.32	19.8	0.688
4		30	109.06	19.2	0.667
5		40	103.80	19.0	0.660
6	Moderate temperature (M-T) group	10	123.61	22.4	0.778
7		20	104.73	15.2	0.528
8		30	97.96	15.5	0.538
9		40	96.30	11.3	0.392
10	High temperature (H-T) group	4	64.38	15.8	0.549
11		8	51.43	8.6	0.297
12		12	42.11	6.6	0.230

$$K_r = \frac{E_n}{E_0}, \tag{5}$$

where K_r is the relative elastic modulus and E_n and E_0 are dynamic elastic modulus of the rock specimen after 0 and n H-C cycle numbers, respectively.

Table 2 and Figure 9(b) illustrate the variation in elastic modulus and K_r of sandstone with different cycling numbers. For the L-T group, K_r decreases to 0.688 after 20 cycles, and then, it has a slight reduction from 20 to 40 cycles. In addition, K_r for the M-T group is larger than that for the L-T group, and after 30 H-C cycles, the values of K_r are 0.667 and 0.538 for L-T and M-T groups, respectively. However, the elastic modulus of the specimen for the H-C group has a larger descent rate after 8 cycles, and the corresponding value of K_r decreases from 1 to 0.297. The decrease trend of the H-T group is obviously larger than that of L-T and M-T groups.

3.4. Variation in Damage. Using damage mechanics methods to study questions of rock hydrothermal coupling is a new development in rock mechanics. The damage variable can describe the deformation and failure degree of the sandstone specimen after different H-C cycles. Two defined methods are adopted and compared in this research to describe the damage degree of sandstone after H-C cycles. Various changes occur in the internal structural of rocks after the H-C cycle, which affect the refraction and diffraction phenomena of ultrasonic propagation. Hence, there has a relationship between wave velocity and damage degree of rock after the H-C cycle. Based on this, damage variable is defined by the variation of longitudinal wave velocity [32]:

$$D_p = 1 - \left(\frac{V_n}{V_0}\right)^2, \tag{6}$$

where D_p stands for damage variable calculated by variation of wave velocity, V_n is the P-wave velocity after n H-T cycle numbers, and V_0 is the P-wave velocity of rock without H-C cycles.

The other effective calculation method to describe the damage variable is based on the variation of dynamic strength [18], which can be calculated according to equation (3):

$$D_\sigma = 1 - \left(\frac{\sigma_n}{\sigma_0}\right), \tag{7}$$

where D_σ stands for the damage variable calculated by variation of dynamic strength, σ_n is the dynamic compressive strength after H-T cycle, and σ_0 is the dynamic compressive strength of the specimen without the H-C cycle.

In addition, the release rate of damage strain energy can describe the damage degree inside rock. The relation between damage and release rate of damage strain energy can be expressed as [33]

$$\theta = \frac{\sigma^2}{2E(1-D)^2}, \tag{8}$$

where θ is the release rate of damage strain energy, σ is the dynamic compressive strength, E is the elastic modulus, and D is the damage variable of rock caused by H-C cycles.

The calculated results of damage variable and release rate of damage strain energy of sandstone are listed in Table 3 and Figures 10 and 11.

As can be observed from Table 3 and Figures 10 and 11, both the damage variable and release rate of damage strain energy can describe the damage variation tendency of the sandstone specimen after different H-C cycles. However, compared with the release rate of damage strain energy, damage variable can better reflect the damage degree; the reason can be clarified as follows. With the increase of cycling number, the damage variables increased gradually, which was in accordance with the general rule of damage evolution in the L-T group. However, the release rate of damage strain energy shows a first-increase-and-then-decrease tendency, which is inappropriate according to the damage evolution rule. Additionally, from the test results of P-wave velocity, porosity, density, and dynamic strength, it is clearly noticed that 20 cycles are critical point of density for L-T and M-T groups, and 4 cycles is critical point for the H-T group, which is similar to the relationship between damage variable and cycling number, while the turning points are different for release rate of damage strain energy, as shown in Figure 11.

Table 3: Test results on damage of sandstone after H-C cycles.

Test number	Number of sample groups	Cycling number	D_p	D_σ	θ_p (MPa)	θ_σ (MPa)
1	Room temperature	0	0	0	0.356	0.356
2	Low temperature (L-T) group	10	0.091	0.025	0.461	0.400
3		20	0.152	0.160	0.508	0.518
4		30	0.160	0.238	0.439	0.533
5		40	0.184	0.275	0.426	0.539
6	Moderate temperature (M-T) group	10	0.087	0.137	0.409	0.458
7		20	0.217	0.268	0.588	0.673
8		30	0.263	0.316	0.570	0.662
9		40	0.285	0.327	0.803	0.906
10	High temperature (H-T) group	4	0.653	0.550	1.089	0.648
11		8	0.751	0.641	2.48	1.193
12		12	0.775	0.706	2.654	1.554

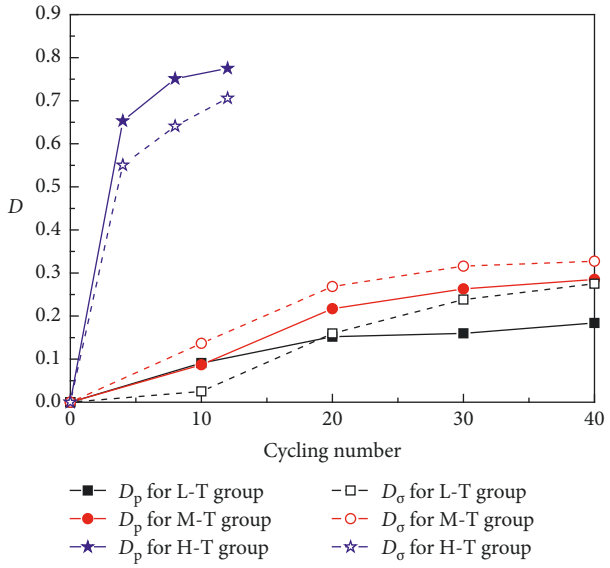

Figure 10: Relation of damage variable with cycling number.

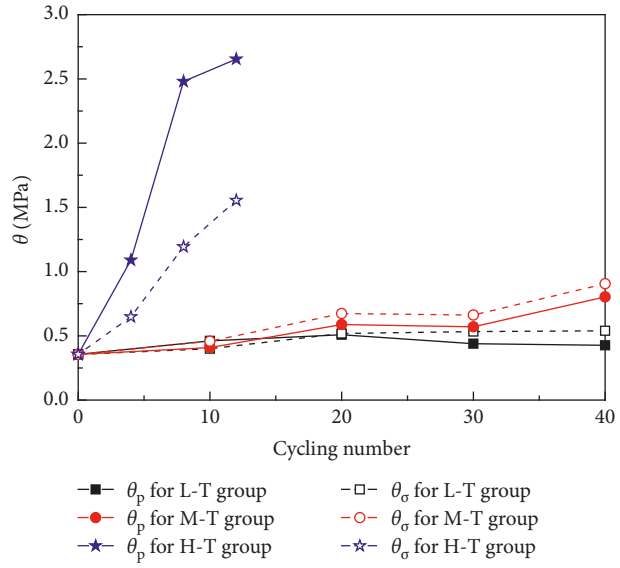

Figure 11: Relation of release rate of damage strain energy with cycling number.

The sandstone used in the tests was a typical sedimentary rock with some original pores and cracks in Figure 2. After repeated action of water and temperature, various internal damage degrees happens inside rock, and the main reasons are as follows:

(1) Repeated erosion of water is one of the causes of rock damage after H-C cycles. On the saturated process, there are original cracks and pores in the rock, as shown in Figure 1. In the process of water absorption, many minerals are hydrophilic and soluble, which promote the weathering of rocks [13, 34–36]. The frequent freezing and thawing of pore water inside rock expands the cracks and pores and promotes the development of new microfractures [7, 11, 37].

(2) Rock specimens are taken out after heat treatment at 50°C, 100°C, and 400°C. The different states of water (attached water, bound water, and mineral combined water) existing inside the rock will evaporate after heat treatment. Particularly, the weakly bound water can completely escape at about 150°C, and the strong bound water can completely escape only at the temperature of about 200°C to 300°C. The crystalline water evaporates and escapes at least 400°C. The loss of component water and crystalline water will lead to the destruction of the crystal structure of sandstone mineral [14, 21].

(3) Because of various thermal expansion coefficients of mineral composition in rock, induced thermal stress between crystal and fissure leads to flaw and exfoliation of rock after heat treatment [32, 33]. After 400°C, the fissures between the crystalline grains in the interior of rocks shows a cracking phenomenon, and the crack cannot be recovered [38, 39].

3.5. Fracture of Sandstone. In order to further illuminate the fracture characteristic of sandstone after the H-C cycle, the fracture result is quantified by mass fractal dimension of fragmentation. The rock fragments are collected and screened by different sizes after the SHPB test. The sizes are 0.15 mm, 0.3 mm, 0.6 mm, 1.18 mm, 2.36 mm, 4.75 mm, 9.5 mm,

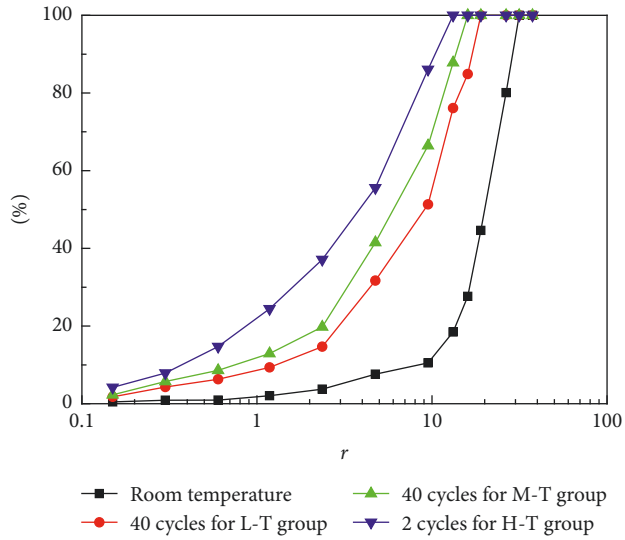

Figure 12: Typical grading curves of rock specimen.

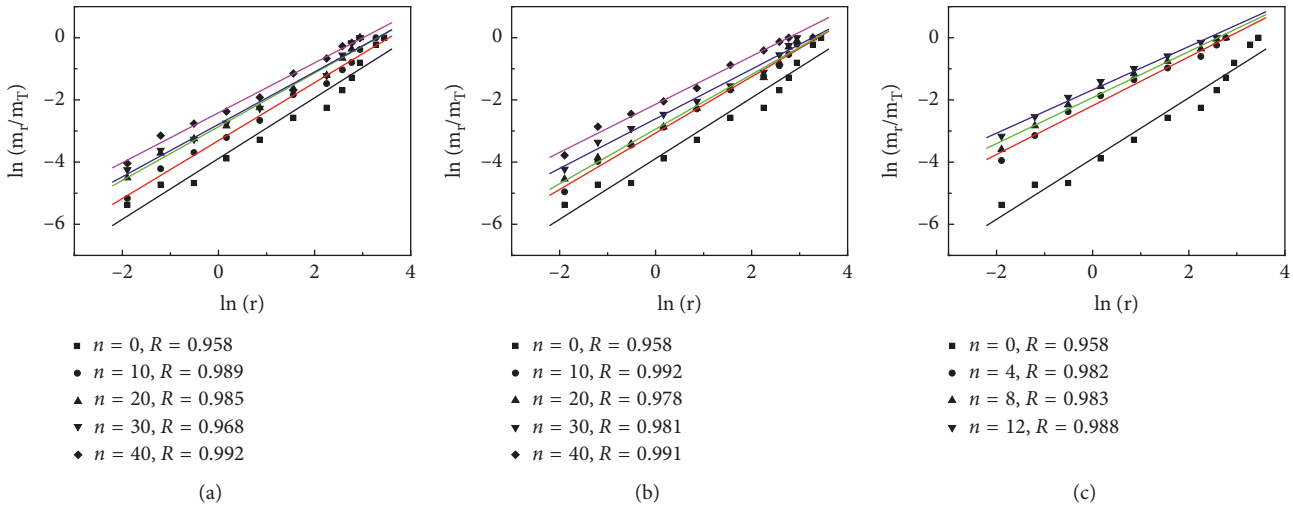

Figure 13: b value of mass fractal dimension of fragmentation: (a) L-T group, (b) M-T group, and (c) H-T group.

13.2 mm, 16 mm, 19 mm, 26.5 mm, 31.5 mm, and 37.5 mm, and the typical grading curves are illustrated in Figure 12.

The mass fractal dimension of fragmentation (D_f) under different test conditions is calculated. The fragment distribution parameter can be calculated by the following formulas [40]:

$$\frac{m_r}{M} = \left(\frac{r}{r_m}\right)^b, \tag{9}$$

$$b = \frac{\ln\left(m_r/M\right)}{\ln r}, \tag{10}$$

where m_r is the accumulative mass under sieve of characteristic size r, M is the total mass of the specimen, r_m is the particle size, and b is the fragment distribution parameter.

The b value is obtained from mass fractal dimension of fragmentation by Formula (10). As shown in Figure 13, with the increase of cycling number, the value of b decreases and the degree of fragmentation increases. The mass fractal dimension of fragmentation is calculated by the following equation:

$$D_f = 3 - b, \tag{11}$$

where D_f is the mass fractal dimension of fragmentation.

The relationship between D_f and cycling number is shown in Figure 14. With the increase of cycling number, the destruction degree of sandstone becomes greater, and the corresponding fragments show more evenly. As seen from Figure 14, the D_f of sandstone ranges from 2.024 to 2.304 under different test conditions in this research. The values of D_f of sandstone increase with increasing cycling number; furthermore, there is a linear relation between mass fractal dimension and cycling number for the L-T group and M-T group, while it exhibits an exponential relation for the H-T

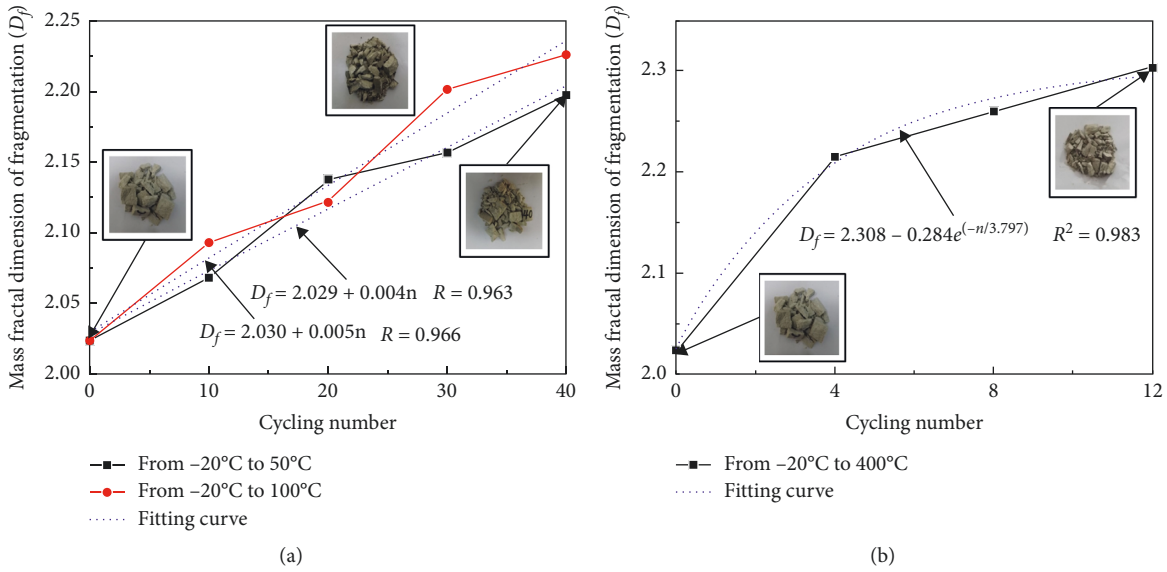

Figure 14: Relation of mass fractal dimension of fragmentation with cycling number. (a) L-T group and M-T group and (b) H-T group.

group. The larger the mass fractal dimension of fragmentation is, the finer the fragmentation is. From the above analysis, it can be noticed that the cycling process promotes the degradation inside the rock specimen, and there exhibits a positive correlation between damage degree and D_f, agreeing with the previous studies results [41, 42].

4. Conclusions

(1) With the increase of cycling number, the P-wave velocity and density decrease, while the porosity increases. Additionally, 20 cycles is critical point of P-wave velocity for the L-T group and M-T group, and 4 cycles is critical point for the H-T group. Both the dynamic compressive strength and K_r decrease with increasing cycling number for three groups, and the descent rate of them is relatively lower for L-T and M-T groups compared with that for the H-T group under the same cycling number.

(2) The damage degree of rock increases with the increase of cycling number. Compared with the release rate of damage strain energy, the damage variable can better describe the damage degree of sandstone after the H-C cycle.

(3) The D_f of sandstone increase with increasing cycling number; furthermore, there has a linear relation between mass fractal dimension and cycling number for the L-T group and M-T group, while it exhibits an exponential relation for the H-T group. The larger the mass fractal dimension of fragmentation is, the finer the fragmentation is.

Data Availability

The datasets generated and analyzed during the current study are available from the corresponding author on reasonable request.

Conflicts of Interest

The authors declare that there are no conflicts of interest regarding the publication of this paper.

Acknowledgments

The work was financially supported by the National Natural Science Foundation of China (no. 51774011), Anhui Provincial Natural Science Foundation (no. 1808085QE148), Project funded by China Postdoctoral Science Foundation (no. 2018M642504), Natural Science Research Project of Colleges and Universities in Anhui Province (no. KJ2017A097), Young Teacher Science Research Project of Anhui University of Science and Technology (no. QN201607), and Doctoral Fund Project of Anhui University of Science and Technology (no. 11674).

References

[1] K. Hall and M.-F. André, "New insights into rock weathering from high-frequency rock temperature data: an Antarctic study of weathering by thermal stress," *Geomorphology*, vol. 41, no. 1, pp. 23–35, 2001.

[2] S. V. Alavi Nezhad Khalil Abad, E. T. Mohamad, and I. Komoo, "Dominant weathering profiles of granite in southern Peninsular Malaysia," *Engineering Geology*, vol. 183, pp. 208–215, 2014.

[3] M. H. Ghobadi and R. Babazadeh, "Experimental studies on the effects of cyclic freezing-thawing, salt crystallization, and thermal shock on the physical and mechanical characteristics of selected sandstones," *Rock Mechanics and Rock Engineering*, vol. 48, no. 3, pp. 1001–1016, 2015.

[4] G. Khanlari and Y. Abdilor, "Influence of wet-dry, freeze-thaw, and heat-cool cycles on the physical and mechanical properties of Upper Red sandstones in central Iran," *Bulletin of Engineering Geology and the Environment*, vol. 74, no. 4, pp. 1287–1300, 2015.

[5] K. Hall and C. E. Thorn, "Thermal fatigue and thermal shock in bedrock: an attempt to unravel the geomorphic processes and products," *Geomorphology*, vol. 206, no. 206, pp. 1–13, 2014.

[6] S. Demirdag, "Effects of freezing-thawing and thermal shock cycles on physical and mechanical properties of filled and unfilled travertines," *Construction and Building Materials*, vol. 47, pp. 1395–1401, 2013.

[7] H. Jiang, Z. Mo, X. Hou, and H. Wang, "Association rules between the microstructure and physical mechanical properties of rock-mass under coupled effect of freeze-thaw cycles and large temperature difference," *Sains Malaysiana*, vol. 46, no. 11, pp. 2215–2221, 2017.

[8] M. Yavuz çelik, "Water absorption and P-wave velocity changes during freeze-thaw weathering process of crosscut travertine rocks," *Environmental Earth Sciences*, vol. 76, no. 12, p. 409, 2017.

[9] H. Yavuz, "Effect of freeze-thaw and thermal shock weathering on the physical and mechanical properties of an andesite stone," *Bulletin of Engineering Geology and the Environment*, vol. 70, no. 2, pp. 187–192, 2011.

[10] A. Kellerer-Pirklbauer, "Potential weathering by freeze-thaw action in alpine rocks in the European Alps during a nine year monitoring period," *Geomorphology*, vol. 296, pp. 113–131, 2017.

[11] S. Huang, Q. Liu, A. Cheng, and Y. Liu, "A statistical damage constitutive model under freeze-thaw and loading for rock and its engineering application," *Cold Regions Science and Technology*, vol. 145, pp. 142–150, 2018.

[12] H. Fu, J. Zhang, Z. Huang, Y. Shi, and W. Chen, "A statistical model for predicting the triaxial compressive strength of transversely isotropic rocks subjected to freeze-thaw cycling," *Cold Regions Science and Technology*, vol. 145, pp. 237–248, 2018.

[13] Q. Sun, C. Lü, L. Cao, W. Li, J. Geng, and W. Zhang, "Thermal properties of sandstone after treatment at high temperature," *International Journal of Rock Mechanics and Mining Sciences*, vol. 85, pp. 60–66, 2016.

[14] W. Zhang, Q. Sun, S. Hao, J. Geng, and C. Lv, "Experimental study on the variation of physical and mechanical properties of rock after high temperature treatment," *Applied Thermal Engineering*, vol. 98, pp. 1297–1304, 2016.

[15] C. Zhou, Z. Wan, Y. Zhang, and B. Gu, "Experimental study on hydraulic fracturing of granite under thermal shock," *Geothermics*, vol. 71, pp. 146–155, 2018.

[16] Y. B. Wang, "Rock dynamic fracture characteristics based on NSCB impact method," *Shock and Vibration*, vol. 2018, Article ID 3105384, 13 pages, 2018.

[17] W. Wang, H. Wang, D. Y. Li, H. M. Li, and Z. M. Liu, "Strength and failure characteristics of natural and water-saturated coal specimens under static and dynamic loads," *Shock and Vibration*, vol. 2018, Article ID 3526121, 15 pages, 2018.

[18] Q. Ma, D. Ma, and Z. Yao, "Influence of freeze-thaw cycles on dynamic compressive strength and energy distribution of soft rock specimen," *Cold Regions Science and Technology*, vol. 153, pp. 10–17, 2018.

[19] P. Wang, J. Xu, S. Liu, H. Wang, and S. Liu, "Static and dynamic mechanical properties of sedimentary rock after freeze-thaw or thermal shock weathering," *Engineering Geology*, vol. 210, pp. 148–157, 2016.

[20] Y. Xu and F. Dai, "Dynamic response and failure mechanism of brittle rocks under combined compression-shear loading experiments," *Rock Mechanics and Rock Engineering*, vol. 51, pp. 743–746, 2018.

[21] H.-b. Du, F. Dai, Y. Xu, Y. Liu, and H.-n. Xu, "Numerical investigation on the dynamic strength and failure behavior of rocks under hydrostatic confinement in SHPB testing," *International Journal of Rock Mechanics and Mining Sciences*, vol. 108, pp. 43–57, 2018.

[22] X. Liu, S. Yuan, Y. Sieffert, S. Fityus, and O. Buzzi, "Changes in mineralogy, microstructure, compressive strength and intrinsic permeability of two sedimentary rocks subjected to high-temperature heating," *Rock Mechanics and Rock Engineering*, vol. 49, no. 8, pp. 2985–2998, 2016.

[23] Q.-L. Ding, F. Ju, X.-B. Mao, D. Ma, B.-Y. Yu, and S.-B. Song, "Experimental investigation of the mechanical behavior in unloading conditions of sandstone after high-temperature treatment," *Rock Mechanics and Rock Engineering*, vol. 49, no. 7, pp. 2641–2653, 2016.

[24] ISRM, *The Complete ISRM Suggested Methods for Rock Characterization, Testing and Monitoring*, R. Ulusay and J. Hudson, Eds., pp. 1974–2006, International Society for Rock Mechanics, Salzburg, Austria, 2007.

[25] S. M. Wang, L. J. Dong, and J. Zhou, "Influence of early age on the wave velocity and dynamic compressive strength of concrete based on split Hopkinson pressure bar tests," *Shock and Vibration*, vol. 2018, Article ID 8206287, 8 pages, 2018.

[26] Y. X. Zhou, K. Xia, X. B. Li et al., "Suggested methods for determining the dynamic strength parameters and mode-I fracture toughness of rock materials," *International Journal of Rock Mechanics and Mining Sciences*, vol. 49, pp. 105–112, 2012.

[27] F. Dai, Y. Xu, T. Zhao, N.-w. Xu, and Y. Liu, "Loading-rate-dependent progressive fracturing of cracked chevron-notched Brazilian disc specimens in split Hopkinson pressure bar tests," *International Journal of Rock Mechanics and Mining Sciences*, vol. 88, pp. 49–60, 2016.

[28] H. Du, F. Dai, K. Xia, N. Xu, and Y. Xu, "Numerical investigation on the dynamic progressive fracture mechanism of cracked chevron notched semi-circular bend specimens in split Hopkinson pressure bar tests," *Engineering Fracture Mechanics*, vol. 184, pp. 202–217, 2017.

[29] Y. Xu, F. Dai, N. W. Xu, and T. Zhao, "Numerical investigation of dynamic rock fracture toughness determination using a semi-circular bend specimen in split Hopkinson pressure bar testing," *Rock Mechanics and Rock Engineering*, vol. 49, no. 3, pp. 731–745, 2016.

[30] S. Liu and J. Xu, "An experimental study on the physico-mechanical properties of two post-high-temperature rocks," *Engineering Geology*, vol. 185, pp. 63–70, 2015.

[31] Y. Zhang, Q. Sun, L. Cao, and J. Geng, "Pore, mechanics and acoustic emission characteristics of limestone under the influence of temperature," *Applied Thermal Engineering*, vol. 123, pp. 1237–1244, 2017.

[32] J. Chen, S. Ren, C. Yang, D. Jiang, and L. Li, "Self-healing characteristics of damaged rock salt under different healing conditions," *Materials*, vol. 6, no. 8, pp. 3438–3450, 2013.

[33] R. R. Zhang, L. W. Jing, and Q. Y. Ma, "Experimental study on thermal damage and energy evolution of sandstone after high temperature treatment," *Shock and Vibration*, vol. 2018, Article ID 3845353, 2018.

[34] B. Liu, Y. Ma, G. Zhang, and W. Xu, "Acoustic emission investigation of hydraulic and mechanical characteristics of muddy sandstone experienced one freeze-thaw cycle," *Cold Regions Science and Technology*, vol. 151, pp. 335–344, 2018.

[35] Z. Zhou, X. Cai, L. Chen, W. Cao, Y. Zhao, and C. Xiong, "Influence of cyclic wetting and drying on physical and dynamic compressive properties of sandstone," *Engineering Geology*, vol. 220, pp. 1–12, 2017.

[36] Y.-H. Huang, S.-Q. Yang, W.-L. Tian, J. Zhao, D. Ma, and C.-S. Zhang, "Physical and mechanical behavior of granite containing pre-existing holes after high temperature treatment," *Archives of Civil and Mechanical Engineering*, vol. 17, no. 4, pp. 912–925, 2017.

[37] F. Gao, Q. Wang, H. Deng et al., "Coupled effects of chemical environments and freeze-thaw cycles on damage characteristics of red sandstone," *Bulletin of Engineering Geology and the Environment*, vol. 76, no. 4, pp. 1481–1490, 2017.

[38] S. Chen, C. Yang, and G. Wang, "Evolution of thermal damage and permeability of Beishan granite," *Applied Thermal Engineering*, vol. 110, pp. 1533–1542, 2017.

[39] X. G. Zhao, Z. Zhao, Z. Guo et al., "Influence of thermal treatment on the thermal conductivity of Beishan granite," *Rock Mechanics and Rock Engineering*, vol. 51, no. 7, pp. 2055–2074, 2018.

[40] B. Kong, E. Wang, Z. Li et al., "Electromagnetic radiation characteristics and mechanical properties of deformed and fractured sandstone after high temperature treatment," *Engineering Geology*, vol. 209, pp. 82–92, 2016.

[41] G. L. Li, L. Y. Wei, H. J. Su, H. W. Jing, and T. Zhang, "Dynamic properties of corroded limestone based on SHPB," *Chinese Journal of Rock Mechanics and Engineering*, vol. 37, no. 9, pp. 2075–2083, 2018.

[42] R. R. Zhang and L. W. Jing, "Analysis on the fragment and energy dissipation of deep sandstone after high/low temperature treatment in SHPB tests," *Journal of China Coal Society*, vol. 43, no. 7, pp. 1884–1892, 2018.